


RESEARCH ARTICLE

Fog type classification using a modified Richardson number for Christchurch, New Zealand

Dongqi Lin^{1,2}  | Marwan Katurji² | Laura E. Revell¹ | Basit Khan³ | Neal Osborne⁴ | Iman Soltanzadeh⁴ | Stefanie Kremser⁵

¹School of Physical and Chemical Sciences, University of Canterbury, Christchurch, New Zealand

²School of Earth and Environment, University of Canterbury, Christchurch, New Zealand

³Institute of Meteorology and Climate Research, Atmospheric Environmental Research (IMK-IFU), Karlsruhe Institute of Technology (KIT), Garmisch-Partenkirchen, Germany

⁴Meteorological Service of New Zealand Limited, Wellington, New Zealand

⁵Bodeker Scientific, Alexandra, New Zealand

Correspondence

Dongqi Lin, School of Physical and Chemical Sciences, University of Canterbury, Christchurch, New Zealand.
Email: dongqi.lin@pg.canterbury.ac.nz

Funding information

Bundesministerium für Bildung und Forschung, Grant/Award Numbers: 01LP1601A, 01LP1911H; Ministry of Business, Innovation and Employment, Grant/Award Number: BSCIF1802; Royal Society Te Apārangi, Grant/Award Number: RDF-UOC1701

Abstract

Situated on a coastal plain between the Southern Alps and Banks Peninsula, Christchurch, New Zealand, experiences around 49 fog days every year. Given its complex topography, accurate fog forecasting is difficult at Christchurch International Airport (CHA). Climatological analysis of local fog events is an important first step to gain insight into the processes involved in the fog life-cycle. In this study, fog events were identified using 12 years of meteorological observations from an automatic weather station situated at CHA. A novel fog type classification method was developed using the modified Richardson number (*MRi*). The *MRi* fog type classification method assesses the local dynamic stability of a 1.25 m shallow layer of near-surface air. Here, the *MRi* is used as a quantitative index to classify advection fog, advection–radiation fog, and radiation fog. Vertical gradients of air temperature and wind speed were derived for pre-fog and fog periods, and a number of criteria were applied to the *MRi* for the fog type classification. The fog type classification results were examined in correspondence with the derived fog intensity, duration, diurnal and seasonal variability of frequency of occurrences, and synoptic and local wind flows. In agreement with other fog studies across the world, fog occurs most frequently during local winter and spring. Radiation fog is the predominant type of fog identified at CHA, and its formation and development usually coincide with the local drainage northwesterlies. This study is the first to use long-term observational data to investigate the fog climatology and typology at CHA in detail. The fog climatological characteristics presented in this study will serve as the basis of future fog studies in Christchurch. The presented *MRi* fog type classification method can potentially be used in fog characteristic studies worldwide.

KEYWORDS

fog climatology, fog type classification, modified Richardson number

This is an open access article under the terms of the [Creative Commons Attribution](https://creativecommons.org/licenses/by/4.0/) License, which permits use, distribution and reproduction in any medium, provided the original work is properly cited.

© 2022 The Authors. *International Journal of Climatology* published by John Wiley & Sons Ltd on behalf of Royal Meteorological Society.

1 | INTRODUCTION

Fog is a meteorological phenomenon in the lower atmospheric boundary layer in association with poor visibility. Fog has a considerable impact on human society and safety, such that the related economic losses can be on a similar order of magnitude to winter storms, hurricanes, or tornadoes (Gultepe *et al.*, 2007). In addition, adverse visibility conditions strongly affect traffic flows (Bergot *et al.*, 2015). The physical processes involved in fog development are supported by a wealth of fog-related research, but forecasting fog accurately remains a challenge (e.g., Gultepe *et al.*, 2007, and references therein). While fog occurs in a wide variety of meteorological conditions, the occurrence and development of fog are also highly dependent on the studied site's specific physical and environmental conditions, such as air pollution, land use, topography, and soil moisture and temperature (e.g., Zhang *et al.*, 2013; Bergot *et al.*, 2015; Maronga and Bosveld, 2017; Mazoyer *et al.*, 2017; Smith *et al.*, 2018). Climatological characteristics and statistics of fog at a given location are considered useful to improve the understanding of the nature of fog and subsequently to better predict fog occurrence (e.g., Gultepe *et al.*, 2007; Román-Cascón *et al.*, 2016).

Christchurch (43.5321°S, 172.6362°E; Figure 1) is one of the largest cities in New Zealand. Both Banks Peninsula to the south and the Southern Alps to the northwest have large influences on local mesoscale meteorology in Christchurch. As reported by McKendry (1983), the winds over the Canterbury Plains are strongly modified by the Southern Alps which provide a barrier to the mid-latitude westerlies in the Southern Hemisphere. Also, the northeasterly airflow can be funnelled by Banks Peninsula onto the Canterbury Plains. The westerly cold air from the foothills of the Southern Alps and the winds down the slopes of Banks Peninsula converge and generate stagnant air zones across the city and its rural boundaries. The drainage westerly flows can also enhance the strength of the near-surface temperature inversion (McKendry, 1983; Kossmann and Sturman, 2004). In addition to the coastal ocean, Lake Ellesmere to the south also provides a source of moisture for fog development in Christchurch. Such complexity of the local orography and environment makes accurate fog forecasting difficult at Christchurch. Located within 20 km of the Pacific Ocean, Christchurch International Airport (CHA) is New Zealand's second largest airport and a vital hub for trade, tourism markets, and freight industries. As recorded at CHA, fog occurs on average 49 days per year,

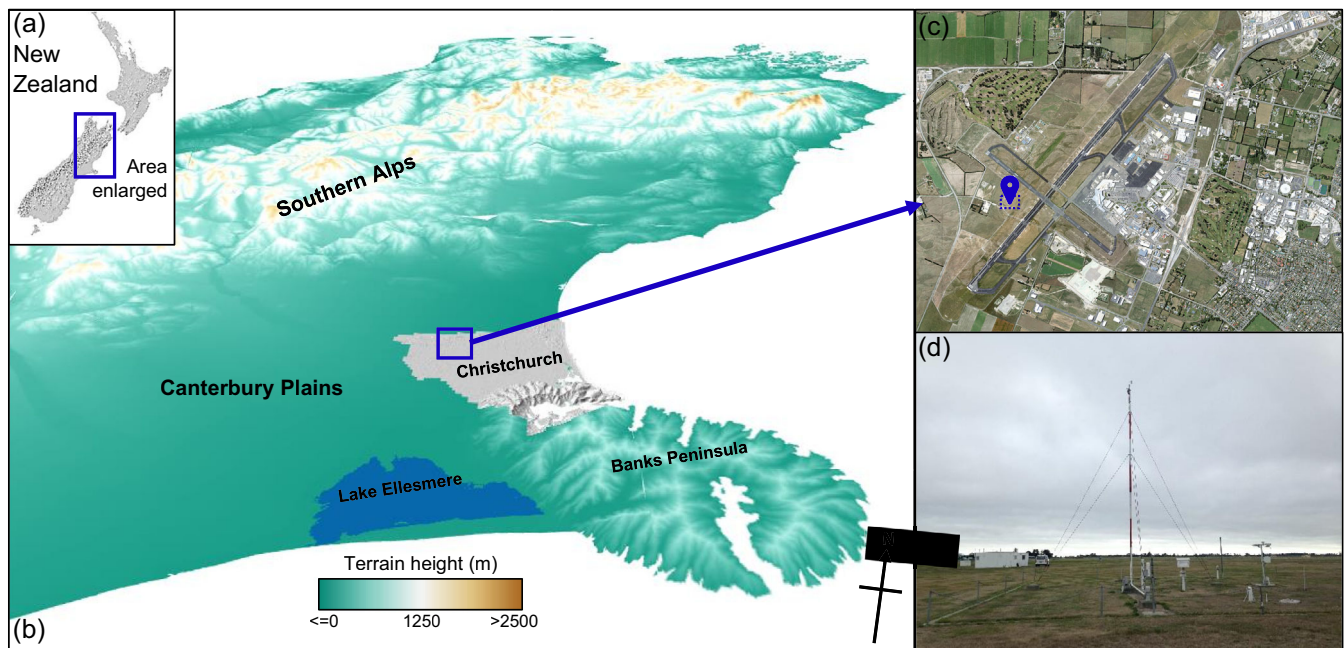


FIGURE 1 Maps and images of the AWS location at CHA, New Zealand: (a) a topographic map of New Zealand, (b) a topographic map of the regions near Christchurch, (c) an aerial photo of CHA, and (d) a picture of the AWS installation location. In panel (b), the major Christchurch area is coloured in grey, and Lake Ellesmere (TeWaihora) is coloured in blue. Map data contain New Zealand North Island and South Island 25 m digital elevation data (, 2018; Landcare Research, 2020a), Christchurch 1 m digital surface data (Environment Canterbury Regional Council, 2020), and the New Zealand land cover database V5.0 (Landcare Research, 2020b). The aerial photos contain data from Land Information New Zealand (2021). Source: AWS image, Meteorological Service of New Zealand Limited (MetService) [Colour figure can be viewed at wileyonlinelibrary.com]

wherein 24 days (49%) are recorded between May and August or austral autumn to late winter (Macara, 2016). Despite the inevitable adverse impact of fog, to the best of our knowledge, no prior studies have investigated fog climatological characteristics in detail at CHA using long-term automatic weather station (AWS) data. The early work of Hume (1999) provided an overview of the fog climatology for several New Zealand airports including CHA, but most of their visibility data were manually recorded and they did not illustrate the climatological characteristics for different fog types. Macara (2016) suggested that Christchurch is mainly affected by advection fog and radiation fog, but did not present any fog type analysis.

Fog type classification using climatological analysis is expected to offer more insight into the processes driving local fog formation than operational forecasting tools (Roux *et al.*, 2021). Tardif and Rasmussen (2007), hereafter TR07, developed comprehensive fog type definitions and an event-based objective classification algorithm for fog climatology and typology in the New York City region of the United States. Their work has since been adopted for many fog studies around the world, such as Cape Town, South Africa (Van Schalkwyk and Dyson, 2013), South Korea (Belorid *et al.*, 2015), Japan (Akimoto and Kusaka, 2015), the Grand Casablanca Region, Morocco (Bari *et al.*, 2016), and Perth, Australia (Roux *et al.*, 2021). These studies emphasized the importance of the surrounding environment in relation to fog development at the studied sites, especially at coastal regions, where onshore flows are responsible for the transport of moisture and subsequently fog development. Advection fog is found to be more frequent around islands, coastal areas, or inland areas near large lakes (e.g., TR07; Belorid *et al.*, 2015).

The event-based method usually uses a fixed wind speed threshold to distinguish advection fog events and radiation fog events (e.g., fig. 4 presented in TR07, and node 1 in fig. 2 presented in Bari *et al.*, 2016) or strong-wind type and weak-wind type (e.g., Akimoto and Kusaka, 2015). A fixed wind speed threshold may lead to incorrect classification of fog events. For example, while an advection fog event reported by Liu *et al.* (2016) is associated with wind speed below $2.5 \text{ m}\cdot\text{s}^{-1}$ during its entire lifecycle (refer to fig. 2 in Liu *et al.*, 2016), a fog event associated with wind speed below $2.5 \text{ m}\cdot\text{s}^{-1}$ is not usually classified as an advection fog event in most of the previous fog type classification studies (e.g., TR07; Akimoto and Kusaka, 2015; Bari *et al.*, 2016; Van Schalkwyk and Dyson, 2013; Roux *et al.*, 2021). Also, as highlighted by Baker *et al.* (2002), the real requirement for radiation fog is lack of turbulence instead of lack of wind because the strength of the nocturnal inversion strongly controls

the wind speed at the surface. Furthermore, a few criteria were not defined quantitatively in previous event-based classification methods. For example, while “cooling prior to onset” is usually used to classify radiation fog events (e.g., TR07; Bari *et al.*, 2016; Roux *et al.*, 2021; Van Schalkwyk and Dyson, 2013), the required temperature gradient of cooling is not specified. When classifying fog events due to cloud base lowering, the magnitude of the lowering is also not quantified. In the illustration of radiation fog classification presented by TR07, “only slight warming leading to onset” was used as a criterion, while the definition of “only slight warming” is ambiguous. In this study, the aim is to present a quantitative method to be used for fog type classification at CHA.

In this study, we conducted a climatological study of fog at CHA. The objectives of this study are (a) to classify fog types, (b) to provide a climatology of fog events, and (c) to identify the climatological characteristics of different fog types in Christchurch. Here the form of the modified Richardson number (*MRi*) introduced by Baker *et al.* (2002) was adapted to assess the dynamic stability of a shallow 1.25 m near-surface layer of the atmosphere to diagnose the dominant drivers of the fog event for fog type classification. The primary drivers leading to radiation fog are the nocturnal radiative cooling of the surface and inversion in association with a stable near-surface layer of the atmosphere (e.g., Gultepe *et al.*, 2007; Price, 2011; Syed *et al.*, 2012; Smith *et al.*, 2018). In contrast, the formation of advection fog is primarily driven by advection of warm moist air over a cooler surface (e.g., Willett, 1928; George, 1951; Gultepe *et al.*, 2007), which requires stronger winds rather than a stable and stagnant near-surface layer of the atmosphere prior to fog formation. The *MRi* fog type classification method classifies fog events into specific types and thereby the climatological characteristics of each fog type are identified.

This article is organized as follows. Section 2 describes the data set and method used to identify fog events from 2007 to 2019 at CHA. Details of the *MRi* fog type classification method are presented in section 3. The classification results are verified by the analysis of the climatological characteristics of fog types presented in section 4, followed by discussions and conclusions outlined in section 5.

2 | DATA SET AND FOG EVENT IDENTIFICATION

2.1 | Data description

This study used 1-min AWS measurements obtained at CHA. The location of the AWS is shown in Figure 1. The

data set covered a 12-year period from 1st October 2007 to 31st July 2019 and was provided by the Meteorological Service of New Zealand Limited (hereafter MetService). As visibility is used as an indicator of fog events, high temporal records of visibility are required. However, most of the AWSs operated across Christchurch either do not measure visibility, only cover a short period of time (less than 5 years), or have been discontinued over 5 years ago. There is only one AWS, which is located at CHA, that provides long data records (over 10 years) of required surface observations at a fine temporal resolution of 1-min in the Christchurch region. As a result, the 1-min observations of ground surface temperature, air temperature at 1.25 m above ground level (AGL), visibility at 1.8 m AGL, cloud base height, and wind speed and direction at 10 m AGL were used to identify fog events and classify fog types. Note that the cloud base height is measured by a ceilometer.

2.2 | Fog event identification algorithm

Depending on the scope of a study, various definitions of fog and different thresholds for visibility have been used (TR07). In this study, we used the World Meteorological Organisation (WMO) definition of fog, which is a phenomenon at the Earth's surface with horizontal visibility reduced to less than 1 km due to suspension of water droplets in the air (e.g., WMO, 1992; Gultepe *et al.*, 2007; TR07). Furthermore, we only focus on fog events with adverse visibility conditions lasting more than 1 hr. Subsequently, short-lived, patchy and not well-established fog events are excluded from the analysis. These fog events should be avoided for robust statistical analysis (Román-Cascón *et al.*, 2016). MetService has provided a record of daily fog occurrences between 1st January 2010 and 1st January 2020, and the universal time coordinated (UTC) date is used. However, the time of fog onset, event duration, and fog types are not recorded. Their daily records only include information on whether fog occurred, fog was significant to aviation, or mist occurred.

The MetService reports a mist event when visibility is at least 1 km but not more than 5 km, following the definition stated by International Civil Aviation Organization (ICAO, 2018). It should be noted that various fog and mist events are reviewed by a number of various individual forecasters at MetService. In contrast, we developed an objective fog identification algorithm to (a) avoid potential biases in subjective interpretations of fog events and (b) provide references of onset time, duration, and dissipation time for each fog event. The fog days reported by MetService are used as a reference to examine the performance of the identification algorithm described below.

A schematic of the fog identification algorithm is shown in Figure 2. The fog events are identified on a daily basis with time in UTC instead of New Zealand standard time (NZST), that is, 0000 UTC is equivalent to 1200 NZST. We define a 24-hr period from 0000 to 2359 UTC as one UTC day. The UTC day covers the entire nocturnal period at CHA. In Christchurch, fog usually forms nocturnally and rarely extends to the afternoon. Therefore, the daily analysis in UTC can capture the fog lifecycle for most of the fog events without interruption. Also, the identified fog days with UTC as a time reference can be validated against the MetService records. The 1-min AWS data were processed into 5-min averages which are sufficient to filter noise in the measurements, and provide an adequate number of samples for statistical analysis.

For each UTC day, the algorithm first looks for periods with visibility less than 1 km. If the visibility was greater than 1 km during the entire day, that day is marked as not a fog day. For each timestamp with visibility less than 1 km, the algorithm calculates the mean visibility for the 1 hr immediately after the timestamp. If the 1-hr mean visibility is less than 1 km, then the first timestamp of the day that satisfies this criterion is marked as fog onset (t_{s_0}). All the periods with visibility less than 1 km after t_{s_0} are marked as potential fog periods. The 3 hr immediately before t_{s_0} are marked as prefog periods. Here, the 3-hr period is used to represent the dynamic meteorological conditions before fog onset. A period longer than 3 hr may include more daylight hours for fog events that occurred in the early evenings. A period shorter than 3 hr may not be sufficient to describe the characteristics of different fog types. The prefog periods are used in the fog type classification described in section 3. If all timestamps with visibility less than 1 km do not have a following 1-hr average visibility less than 1 km, then the day is marked as not a fog day. In most fog events, the visibility can decrease to less than 200 m. The 1 km threshold of the 1-hr mean is used to include fog events with a patchy start during which the observed visibility may be above 1 km for a very short period within an hour. In addition, precipitation events could also lead to a reduction of observed visibility. Overall, 514 UTC days within the 12-year analysis period coincided with precipitation and visibility less than 1 km recorded on the same UTC day, but the reduced visibility resulting from these events usually has a duration shorter than 30 min. The 1-hr mean of the observed visibility less than 1 km allows the algorithm to exclude precipitation events. Within the 514 UTC days, the algorithm identified 101 fog events, wherein only nine events were associated with precipitation at fog onset or during fog development. In the other 92 fog events, precipitation

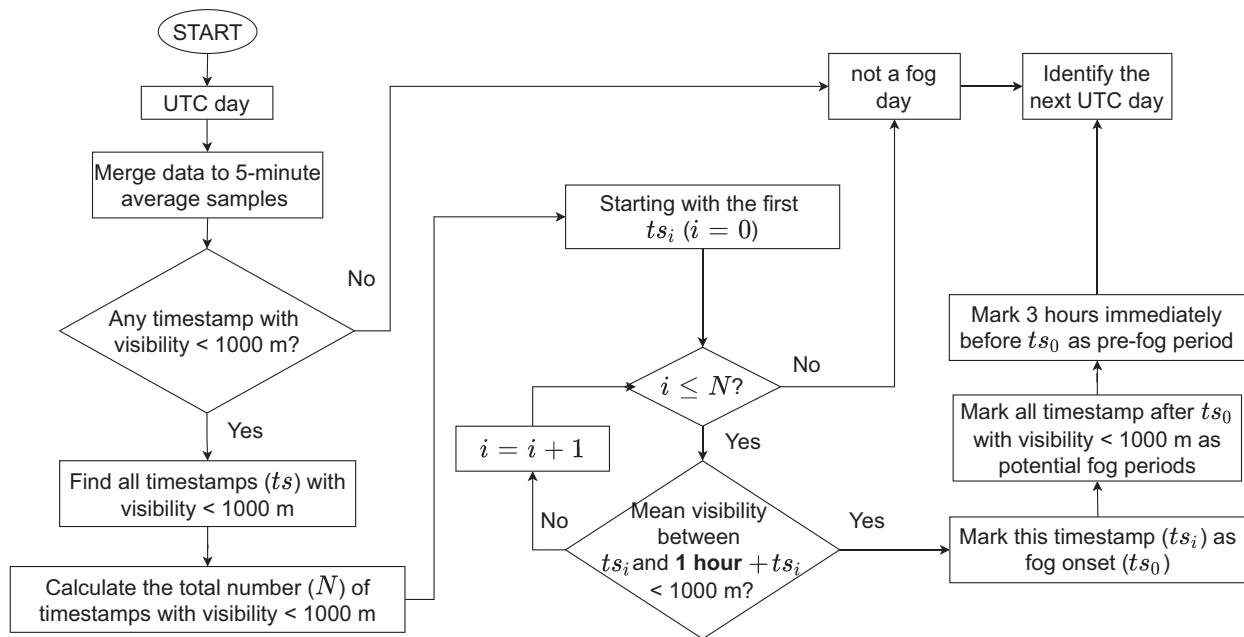


FIGURE 2 Flowchart illustrating the fog event identification algorithm

occurred either a few hours prior to fog formation or after fog dissipated.

2.3 | Validation

The fog events identified by the algorithm were compared to the MetService fog records over the period from 1st January 2010 to 31st July 2019. This period was chosen based on the date range of the 1-min AWS data and the daily fog records provided by MetService. For the entire validation period (3,418 calendar days), 561 fog days were observed by MetService, and the algorithm identified 447 fog days, within which 383 days are recorded as fog days and 28 days are recorded as mist days by MetService. At MetService, a low-visibility event is distinguished and reviewed manually each day, while the identification algorithm does not provide the classification of fog and mist. However, the observed visibility in the 28 mist events reaches the threshold of less than 1 km with their duration exceeding 1 hr, having the potential to further develop into fog. Therefore, these 28 mist events were included as fog events for further analysis. Overall, 91.9% of the fog days identified by the algorithm align with the MetService fog records. Regarding the clear days, the algorithm identified 2,971 clear days, wherein 2,870 days (96.6%) are recorded as a clear day by MetService.

There are several explanations of the missed and false detected fog days by the algorithm. Visibility is the only indicator for fog events used in the algorithm. Manual

investigation shows that most of the missed fog events are relatively short (<1 hr) and only have visibility less than 1 km with a duration less than 30 min during the entire fog period, while the algorithm is designed to exclude such short events. All the 38 false detection events show a reduction in visibility to less than 1 km with a duration of more than 1 hr. Within the false detection events, four events extended from one UTC day to the day after. MetService recognizes such an event as one fog event and only marks the day when fog formation started as a fog day. The algorithm, however, analyses fog events for each day separately, and therefore identifies such events as two separate events.

Given that over 90% of the fog and clear events detected by the algorithm align with the MetService fog records, the identification algorithm is applicable to identify fog events and the identified fog events are therefore used for further analysis described below.

3 | FOG TYPE CLASSIFICATION

3.1 | Fog types

Several studies have established comprehensive fog type definitions (e.g., Willett, 1928; George, 1951; TR07). Here, we follow the guidance of TR07 who described five distinct types of fog:

- Precipitation fog (PCP)
- Radiation fog (RAD)

- Advection fog (ADV)
- Fog resulting from the lowering of cloud base (CBL)
- Morning evaporation fog (EVP)

In addition to the five types defined by TR07, we include advection–radiation fog (ADV–RAD) described by George (1951) who stated ADV–RAD is “one of the biggest sources of confusion to forecasters.” ADV is usually defined as a result of a warm moist air mass advected over a cooler surface by relatively strong wind (e.g., Willett, 1928; Bari *et al.*, 2016; TR07). RAD forms with radiative cooling at the surface under clear skies in stagnant air, and is marked by a surface temperature inversion (Willett, 1928). ADV–RAD fog results from both radiation and advection processes. Its formation is a result of moist air being advected over land from a large water body during the previous daylight hours and radiative cooling later in the day (Ryznar, 1977; Bari *et al.*, 2016). The manual investigation of the observations used in this study revealed that PCP rarely occurs at CHA. Therefore, PCP is not included as a fog type in the analysis. In contrast to other fog types, CBL events are not mainly driven by surface processes, such as surface radiative cooling, surface evaporation, and near-surface advection of air mass. CBL is associated with radiative cooling at cloud top, which destabilizes the cloud layer and subsequently generates top-down turbulent mixing towards the subcloud layer (Pilié *et al.*, 1975). The turbulent eddies transport the radiative cooled air downward. The subcloud layer is continuously cooled by evaporation of settling cloud drops, leading to a lowering of cloud base (e.g., Dupont *et al.*, 2012; Menut *et al.*, 2014). Reduction of horizontal visibility resulting from such top-down processes of the cloud layer is frequently observed at CHA. EVP usually starts to form within 1 hr of sunrise (TR07). During sunrise, the surface is heated faster than the air above, leading to evaporation of surface moisture. The water vapour condenses and suspends in the cooler air above the ground resulting in reduction of visibility. EVP is observed at CHA. Hence, the five types of fog retained in this study are RAD, ADV, ADV–RAD, CBL, and EVP.

3.2 | Classification method

The event-based objective fog type classification algorithm developed by TR07 contains several unquantified criteria. Therefore, in this study, an alternative method to classify fog events at CHA using the *MRI* was developed and is presented. The fog types are classified based on the dominant drivers in fog formation and development. The *MRI* is a quantitative index that provides an evaluation of

the dynamic stability of a shallow near-surface layer of the atmosphere. All types of fog occur at a wide range of dynamic stabilities. This includes the very stable conditions associated with radiative cooling and the slightly turbulent conditions associated with advection processes. The dynamic stability in the lowest layers of the atmosphere during prefog and fog periods is considered as the key to classify fog events into different fog types. This *MRI* fog type classification method is only used to classify fog events that are mainly formed and modified by surface–atmosphere interactions, that is, ADV, RAD, ADV–RAD, and EVP. CBL events are identified following the definition described by TR07 (described below).

The bulk Richardson number (*Ri*) is usually used as a parameter for the categorisation of the dynamic stability of a particular layer of the atmosphere and thus the state of turbulence. *Ri* compares the roles of buoyancy to mechanical or shear forces in a flow (Oke, 2002). *Ri* requires temperatures and winds being measured at the top and bottom of a particular layer that are not provided by the AWS at CHA. Thus, we adopt the form of *MRI* introduced in Baker *et al.* (2002),

$$MRI = \frac{T_{\text{air}} - T_{\text{sfc}}}{u^2} \quad (\text{K m}^{-2} \text{ s}^2). \quad (1)$$

Baker *et al.* (2002) used the *MRI* to forecast boundary layer turbulence and subsequently forecast radiation fog occurrence. For the purpose of fog forecast, T_{air} is the forecast air temperature in the boundary layer (the temperature in the lowest model layer or the third model layer above the surface, whichever is warmer), T_{sfc} is the forecast shelter temperature, and u is the forecast wind speed in the lowest model layer (Colby, 1998; Baker *et al.*, 2002). All these variables were taken from operational forecasting model output provided by the United States National Centers for Environmental Prediction (NCEP) (Colby, 1998). The forecast example presented in Baker *et al.* (2002) showed that their objective and process-oriented approach based on *MRI* is effective for radiation fog forecasting. The *MRI* was later adopted by Syed *et al.* (2012) to investigate the variability of fog over their studied region, wherein they used the forecast near-surface temperature as T_{sfc} . In addition, Syed *et al.* (2012) reported that the spatial pattern and the magnitude of fog occurrence derived by their *MRI*-based fog detection scheme are in good agreement with observations.

In this study, we adopt the form of *MRI* to assess the dynamic stability and turbulence state of the shallow 1.25 m layer of the atmosphere above the ground surface. The *MRI* used here is not for fog forecasting. Rather, the *MRI* is used as a quantitative index to represent the

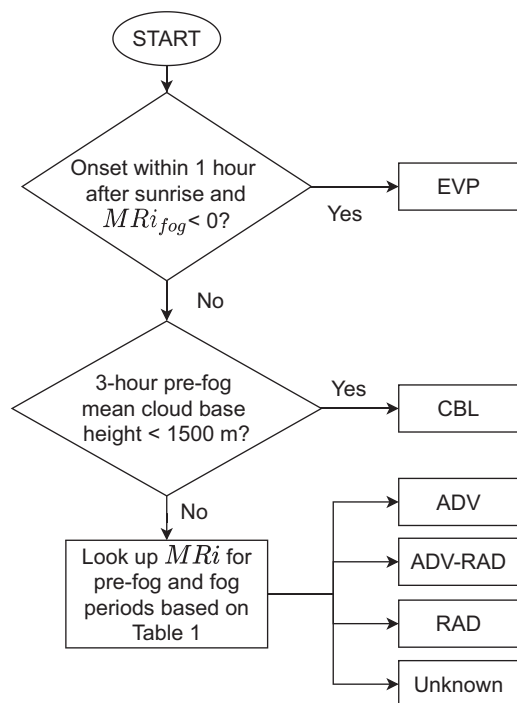


FIGURE 3 Flowchart showing the fog type classification algorithm for morning evaporation fog (EVP), fog resulting from the lowering of cloud base (CBL), advection fog (ADV), advection-radiation fog (ADV-RAD) and radiation fog (RAD)

near-surface layer turbulent mixing and stability. The required temperature and wind data to calculate MRI were obtained from the AWS at CHA, rather than using data from a numerical weather prediction model. Therefore, we use the observed ground surface temperature as T_{sfc} , the observed air temperature at 1.25 m AGL as T_{air} , and the observed wind speed at 10 m AGL as u (in the unit of $m \cdot s^{-1}$). The MRI is derived for both pre-fog ($MRI_{pre-fog}$) and fog (MRI_{fog}) periods identified in section 2. The pre-fog period is considered because it represents the stability leading to fog formation, while the fog period is used to consider whether the stable or unstable conditions sustain throughout the fog lifecycle.

Figure 3 outlines the decision process of the fog type classification. EVP and CBL events are classified independently. EVP events occur within 1 hr of sunrise and result from evaporation of surface water associated with turbulence mixing in the surface layer. Since such evaporation is caused by heating at the surface, EVP events occur with $MRI_{fog} < 0$ ($T_{sfc} > T_{air}$). Furthermore, TR07 identified that an EVP event occurs under calm wind conditions while the cloudiness during the preceding night could be varying. Their research also emphasizes that, as a result of evaporation of surface water, the incoming solar radiation and local surface moisture play the most important roles in EVP events. Therefore, the threshold

of $MRI_{fog} < 0$ and the time of the fog formation are sufficient to represent the EVP event, and the cloud base height and pre-fog conditions are not considered to classify EVP. According to TR07, a CBL event is defined as a fog event resulting from the cloud-base gradually lowering from a height below 1 km within 5 hr prior to fog onset. We follow this definition and define a CBL event as a fog event associated with a mean cloud base height less than 1,500 m within a 3-hr period prior to fog onset. The cloud base height is measured by a ceilometer at CHA, which may only represent the cloud cover conditions over the instrument itself. Large variations in the observed cloud base height may exist in some CBL events. The threshold of 1,500 m is sufficient to include these events, and to prevent the classification method from identifying any other fog types as CBL.

ADV, ADV-RAD, and RAD events are classified using the derived MRI for the pre-fog ($MRI_{pre-fog}$) and fog (MRI_{fog}) periods, and the classification criteria are listed in Table 1. The mean temperatures and wind speed for the pre-fog and fog periods are used to calculate $MRI_{pre-fog}$ and MRI_{fog} .

After intensive testing of the thresholds based on manual inspection of over 200 fog events, $MRI > 1$ is used to represent a strong stable near-surface layer where the turbulence suppressing force of buoyancy dominates. Moderate stability is determined by a threshold of $0.5 < MRI < 1$. Conditions with $0 < MRI < 0.5$ are considered as weak inversion and/or near neutral conditions, wherein T_{air} is greater than T_{sfc} , but either the inversion is weak or wind speed is high and hence turbulence is not suppressed. A negative MRI represents unstable conditions such that the surface is warmer than the overlying air and radiative cooling does not occur at ground surface. These thresholds were examined by the results presented in section 4.

RAD events are considered as fog events in which radiative cooling associated with inversion and a stable near-surface layer is the dominant factor, and the strong stability is sustained throughout the pre-fog and fog periods. $MRI_{pre-fog} > 1$ with $MRI_{fog} > 0$ indicates that a strong inversion develops before fog forms and the inversion sustains. Only $MRI_{fog} > 0$ is used because once fog matures the radiative cooling zone moves to the top of fog. For example, when a RAD event develops into a deep adiabatic radiation fog, radiative cooling primarily occurs at the fog top instead of the surface (Smith *et al.*, 2018). Such a deep adiabatic radiation fog event is usually longer lived, which may lead to a near-zero MRI_{fog} . When a fog event develops in the early evening, the inversion may not be strong during the 3 hr before fog onset ($0.5 < MRI_{pre-fog} < 1$), but a stronger inversion can develop during the fog period ($MRI_{fog} > 1$) where

TABLE 1 Classification of ADV, ADV–RAD, and RAD based on MRI during prefog and fog periods

MRI_{fog}	MRI_{prefog}			
	<0	0–0.5	0.5–1	>1
<0	ADV	ADV	ADV	Unknown
0–0.5	ADV	ADV	ADV	RAD
0.5–1	ADV–RAD	ADV–RAD	ADV–RAD	RAD
>1	ADV–RAD	ADV–RAD	RAD	RAD

Note: Fog events with $MRI_{\text{prefog}} > 1$ and $MRI_{\text{fog}} < 0$ are classified as unknown fog types and are excluded from the fog type classification.

turbulence is suppressed with light wind. In this case, the fog formation is mainly driven by nocturnal radiative cooling and inversion. Hence, such fog events are classified as RAD.

Fog events that do not occur with high stability prior to fog formation and during fog periods are not primarily driven by local radiative cooling. For these fog events, advection is considered as a primary factor for fog formation. Some ADV events could be a fog layer advected from elsewhere, while other ADV events require relatively strong winds to advect warm moist air over the colder land surface (as described by, e.g., TR07; Gulpepe *et al.*, 2007). In ADV events, the strong stability does not sustain throughout the entire prefog and fog periods. As the MRI only assesses the stability locally, the prefog stability for ADV events could vary ($MRI_{\text{prefog}} < 1$). Radiative cooling may still occur in the early evening before the advection fog occurs. However, since the cooling is short-lived, a strong inversion does not develop ($MRI_{\text{prefog}} < 1$). During the fog period, advection is sustained, as it is the dominant factor for ADV events, resulting in an MRI_{fog} value of < 0.5 . Values of $MRI_{\text{fog}} < 0$ indicate unstable conditions, where no temperature inversion is present and the advected air or fog is cooler than the surface. The threshold of $0 < MRI_{\text{fog}} < 0.5$ was chosen to identify ADV because air could be warmer than the land surface following the definition of ADV, while the MRI_{fog} cannot be greater than 0.5 due to the presence of rapid flow coinciding with the advection.

In ADV–RAD events, both the advection of moisture at earlier hours and nocturnal radiative cooling are the primary drivers leading to fog formation and development. When sufficient moisture is advected inland during the previous daylight hours, the dew point temperature is enhanced locally. As a result, less radiative cooling is required for T_{air} to converge to dew point, and an ADV–RAD event usually occurs with a weaker inversion than a RAD event. Therefore, an ADV–RAD event is associated with prefog conditions similar to ADV events ($MRI_{\text{prefog}} < 0.5$), while moderate or strong inversion occurs during fog periods ($MRI_{\text{fog}} > 0.5$). The particular

fog events associated with moderate inversion conditions during both the prefog and fog period ($0.5 < MRI_{\text{prefog}} < 1$ and $0.5 < MRI_{\text{fog}} < 1$) are classified as ADV–RAD. These events are identified as the result of both moderate advection during prefog periods and moderate radiative cooling during fog periods. Without the presence of either process, fog may not form.

The events with $MRI_{\text{prefog}} > 1$ and $MRI_{\text{fog}} < 0$ are not included in the fog type classification. These events rarely occur (only three events recorded at CHA during the entire observational period) and do not show consistent fog characteristics. Thus, they are classified as unknown fog types.

4 | FOG TYPE ANALYSIS

4.1 | Frequency of occurrence

The characteristics of each fog type are examined by duration, diurnal and seasonal variability of fog onset and dissipation times, and the reduced horizontal visibility during the fog event (e.g., TR07; Bari *et al.*, 2016). The seasonal and diurnal variability of fog events are represented using the monthly/diurnal frequency,

$$F_{m,h} = (N_{m,h}/N_{\text{tot}}) \times 100\%, \quad (2)$$

where $F_{m,h}$ is the frequency of fog events at hour h in month m , $N_{m,h}$ is the number of events which occurred at hour h in month m , and N_{tot} is the total number of fog events over the analysis period (TR07). The monthly frequency is

$$F_m = \sum_h F_{m,h} \times 100\%. \quad (3)$$

The hourly frequency is

$$F_h = \sum_m F_{m,h} \times 100\%. \quad (4)$$

4.2 | Fog type characteristics

The seasonal and diurnal frequency distribution of fog events are presented in Figure 4. The frequency is calculated as described in section 4.1. The intensity of each fog type is expressed as the duration and the minimum visibility of each fog event and shown in Figure 5.

As shown in Figure 4a, April and August have the highest frequency of fog events at CHA. Most fog events occur after sunset and dissipate within 2 hr after sunrise. ADV events last the longest among all fog types (Figure 5a). ADV events can extend over 5 hr after sunrise (Figure 4b). Figure 6 compares the frequency distribution of fog events with the variability of daily mean T_{air} and sea surface temperature (SST) in each month. The SST data were obtained from ERA5 data set, the fifth generation of European Centre for Medium-Range Weather Forecasts (ECMWF) atmospheric reanalysis of the global climate (Hersbach *et al.*, 2019). The maximum frequency of ADV is evident in August, while the lowest numbers are in late spring (November) and summer (December and January) (Figure 6a). The peak in August coincides with the lowest SST and a relatively cold boundary layer (Figure 6b). A cold boundary layer is favourable for the fog layer to propagate inland with an onshore push resulting from the northeasterly winds driven by the orography.

ADV–RAD events are frequently observed during the second half of the evenings, especially in spring (March, April, and May) and autumn (September, October, and November; Figure 4c). Similar to ADV events, ADV–RAD events seldom occur in summer. Radiative cooling plays an important role in ADV–RAD events, while boundary layer cooling and reduction of the turbulent mixing during summer nights are usually not sufficient to produce fog. In spring or autumn, the daylight time is still longer than that in winter months; therefore, advection of moisture associated with turbulent mixing during daylight hours hinders the development of sufficient radiative cooling in the first half of the evening. After sunset, with decreasing turbulent mixing during the earlier hours in the evening, a stable layer begins to establish leading to ADV–RAD fog formation in the second half of the evening. With decreasing solar radiation during the day, the boundary layer cools faster in winter months, and therefore ADV–RAD events can occur in the first half of the evening. Although ADV–RAD events are denser than other types of fog with the lowest median of minimum visibility as shown in Figure 5b, they usually dissipate within 1 hr after sunrise (Figure 4c). The increase of solar radiation and subsequently increase of temperature in the boundary layer lead to strengthening of vertical turbulent mixing and a decrease in near-surface relative humidity.

The onset of RAD events shows a strong correlation with sunset time (Figure 4d). RAD events can occur within 2 hr after sunset in winter months and the number increases to 7 hr after sunset in summer months. Similar to ADV–RAD events, RAD events generally dissipate within 1 hr after sunrise. April, July, and August exhibit the highest frequencies of RAD events (Figure 6a) at CHA. These months have relatively long nights to allow the development of radiative cooling, and the surface temperature is not too low, which allows water droplets to be suspended in the atmosphere. June and July are the coldest months at CHA (Figure 6b). When the ground surface is below freezing temperature, the saturation vapour pressure over water is greater than that for ice, and therefore frost is more likely to occur rather than fog (Hume, 1999; Sturman and Tapper, 2006).

EVP events occur within 1 hr of sunrise and most of the events have duration around 2 hr (Figure 4e). Compared with other types of fog, EVP events are short-lived and less dense (Figure 5). Frequencies of EVP events maximize in January and March (Figure 6a). However, over the entire analysis period, only 18 EVP events are identified, which may not provide sufficient samples to represent their characteristics in detail.

In agreement with TR07, the seasonality and diurnal variability in CBL events are less evident compared with other types of fog (Figure 4f). The onset and dissipation time of CBL events still show correlations with sunset and sunrise time, respectively. Similar to ADV–RAD and RAD events, the number of CBL events is greater in late spring and winter months, and is lowest in summer months (Figure 6a). This suggests that boundary layer cooling could still be an important process in CBL events. Although CBL events are less intense regarding reduction of visibility (Figure 5b), they tend to have longer duration (Figure 5a). CBL events could last more than 10 hr, second only to the duration of ADV events.

4.3 | Synoptic and local wind flows

The mean sea level pressure (MSLP) over New Zealand nearest to fog onset for each fog type is shown in Figure 7. The MSLP data were obtained from the ERA5 data set. In general, all fog events at CHA are associated with anticyclonic conditions, while variability exists in the locations of the anticyclone centre. For EVP, CBL, and ADV events, the centre of the high MSLP is located to the east of New Zealand. ADV–RAD events are associated with high MSLP over the North Island, while the centre of the high MSLP is located to the north of the South Island and the west of North Island for RAD events. EVP, CBL, ADV, and ADV–RAD events all show

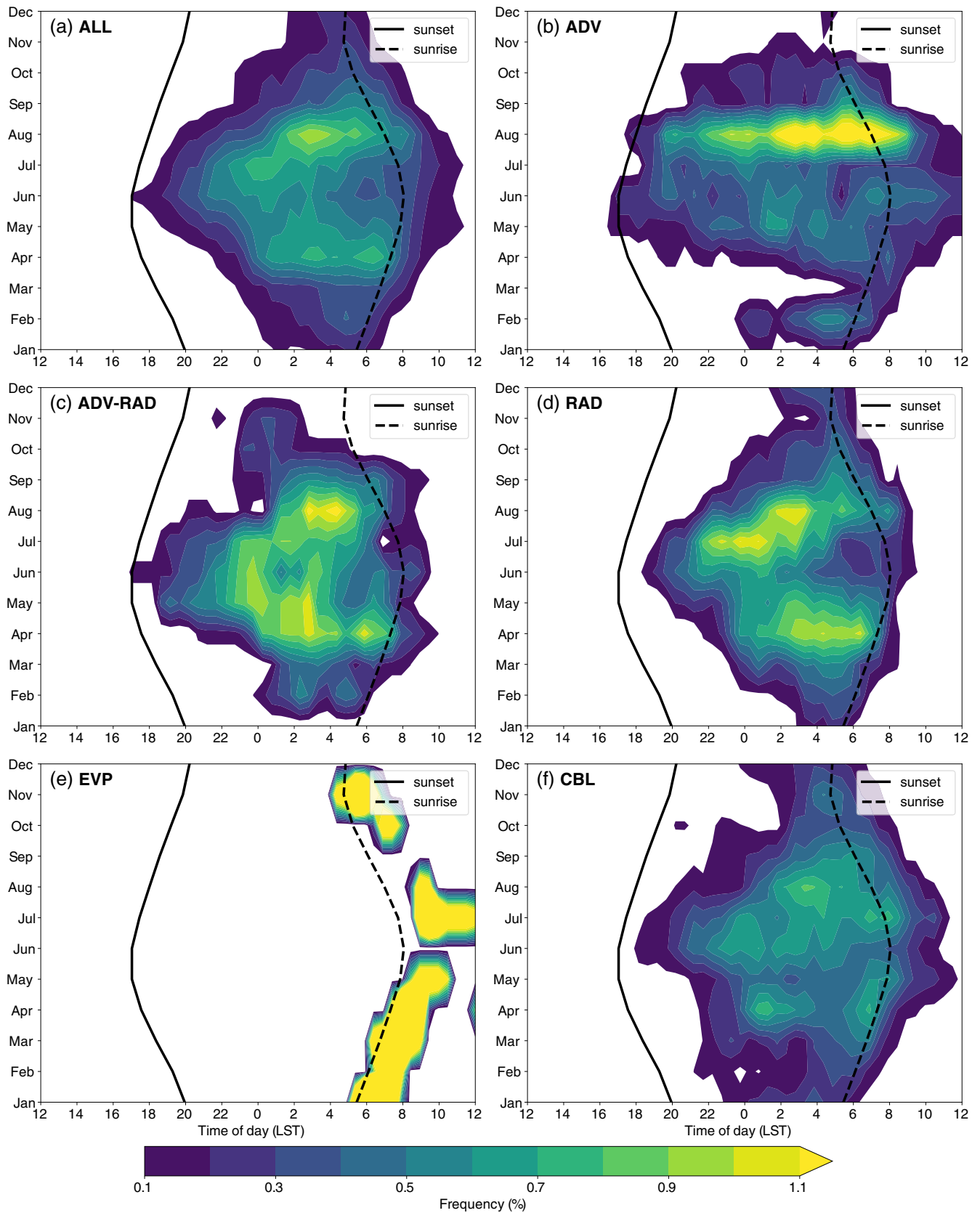


FIGURE 4 Frequency distribution of fog events with respect to time of day and month of the year: (a) all fog events, (b) ADV, (c) ADV-RAD, (d) RAD, (e) EVP, and (f) CBL. The data cover the period between 2007 and 2019. The solid and dotted black lines indicate the sunset and sunrise time, respectively. Data with frequency below 0.1% are not shown. Local standard time (LST) is used [Colour figure can be viewed at wileyonlinelibrary.com]

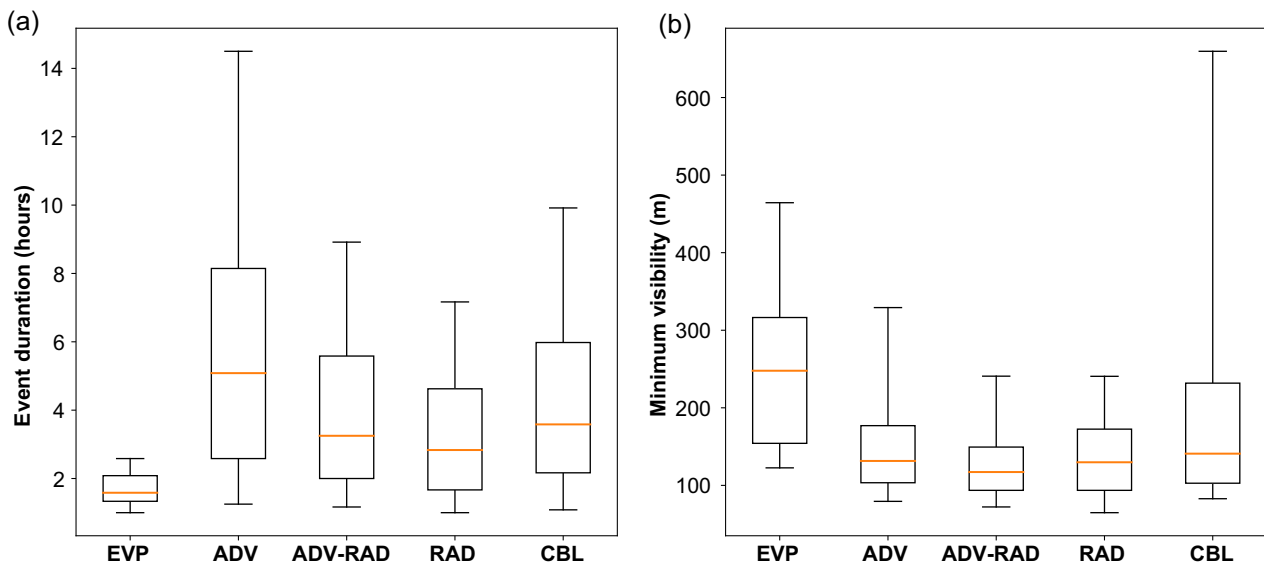


FIGURE 5 Box plots illustrating (a) the fog event duration in hours and (b) minimum visibility observed during each fog event for the five types of fog. The orange line within the box indicates the median. The lower and upper edges of each box represent the 25th and 75th percentiles, respectively. The lower and upper whiskers are the 5th and 95th percentiles, respectively [Colour figure can be viewed at wileyonlinelibrary.com]

zonal flow across the South Island which converges on the Canterbury area resulting in a trough at the lee side of the Southern Alps. The deep orographic lee trough is not observed in RAD events, suggesting clear sky conditions, which is favourable for nocturnal radiative cooling. However, the synoptic analysis failed to capture the variation of local flows, which is modified by the surrounding environment of CHA. The synoptic weather systems are dynamic and fog is very sensitive to the location of synoptic circulations. While the synoptic conditions show subtle difference across most fog events, the local dynamics also vary case by case. Figures 8 and 9 present the frequencies of wind speed and direction for each fog type during prefog and fog periods, respectively. During prefog periods, the dominant wind is northeasterly for all fog events regardless of fog types (Figure 8a), while both the northeasterlies and the northwesterlies have a frequency over 10% in all fog events during fog periods (Figure 9a).

ADV events are associated with southwesterlies and northeasterlies during the prefog periods (Figure 8b). The southwesterlies advect warm moist air or a blanket of fog from Lake Ellesmere, which is located to the southwest of Christchurch (Figure 1). The northeasterlies are due to either the sea breeze or an orographically driven circulation. In contrast to their prefog periods, ADV events during fog periods are associated with a higher frequency of southwesterlies and a lower frequency of northeasterlies (Figure 9b). The evident signal of southwesterlies is likely to be an association with advection of a blanket of fog over CHA. Fog may have formed near Lake Ellesmere before advection occurs.

The prefog periods in ADV–RAD events are mainly associated with northeasterlies (Figure 8c). The north-easterlies are responsible for advection of moist air from the warm ocean, which keeps the dew point high over Christchurch. In contrast to ADV events, ADV–RAD events show a significantly lower ratio of southwesterlies during prefog periods (Figure 8c). Scattered cloud and sometimes overcast conditions are frequently present with southwest winds (Sturman and Tyson, 1981). Such conditions are not favourable to development of radiative cooling, and hence ADV–RAD events rarely occur with southwesterlies. In ADV–RAD events, significant numbers of northwesterlies are observed during fog periods (Figure 9c). In Christchurch, northwesterlies are often associated with the foehn effect, which leads to rapid increases in temperature and wind speed, and decrease in relative humidity (Sturman and Tapper, 2006). Fog is unlikely to form under these conditions. However, as shown in Figure 9c, the wind speed is relatively low (below $2 \text{ m}\cdot\text{s}^{-1}$), which is more likely to be a result of the drainage flow and stagnant air masses as reported by Corsmeier *et al.* (2006). The cold northwesterly drainage flow is associated with a stable boundary layer suggesting the sustenance of radiative cooling during the fog life-cycle, which agrees with the definition of ADV–RAD.

RAD prefog periods show a strong signal of light northwesterlies (Figure 8d), which is considered as an indicator of the drainage flow and a stable boundary layer. During both prefog and fog periods, a greater number of northwesterlies is observed in RAD events than in

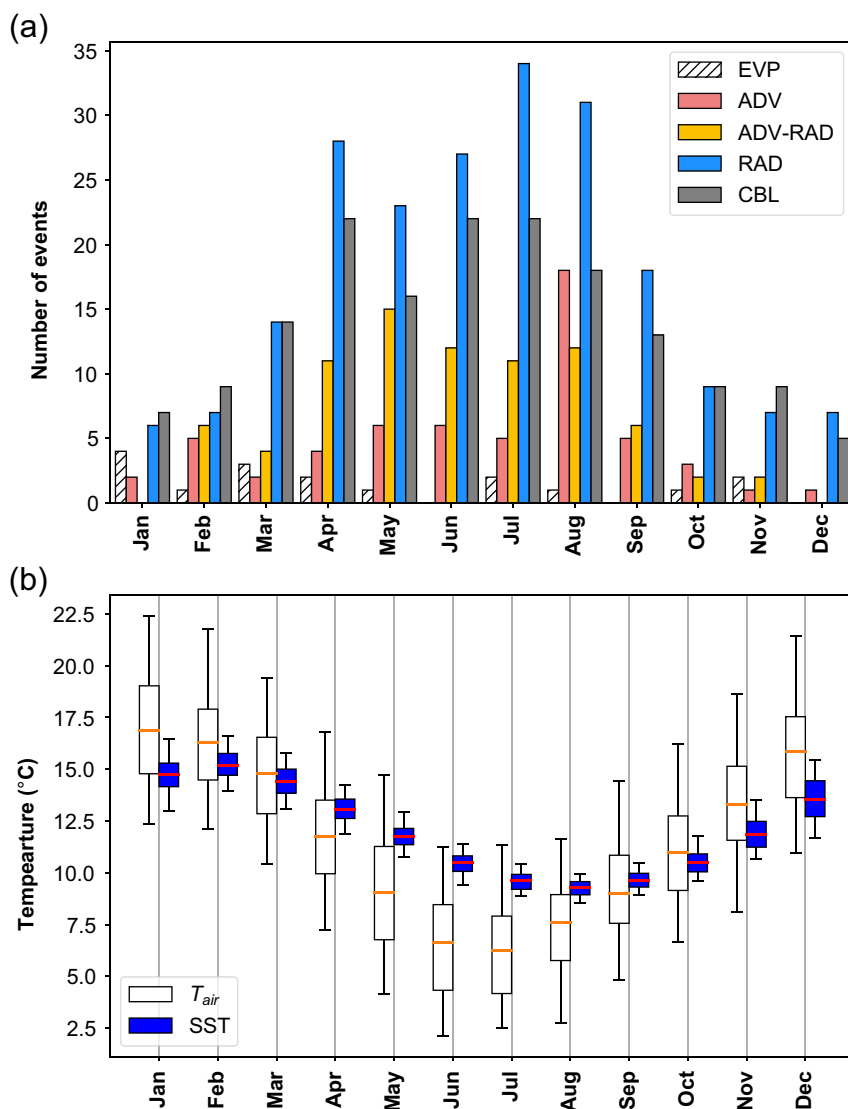


FIGURE 6 (a) The monthly number of events for each fog type. (b) Monthly variability in daily mean air temperature observed at CHA (T_{air}) and the daily SST at the nearest grid points from CHA. The SST data are taken from ERA5 data set (Hersbach *et al.*, 2019) [Colour figure can be viewed at wileyonlinelibrary.com]

ADV–RAD events. This agrees with the definitions of RAD and ADV–RAD. Due to absence of moisture advected from large water bodies, RAD requires stronger radiative cooling and subsequently stronger surface temperature inversion for its formation than ADV–RAD. The northeasterlies in RAD and ADV–RAD events may be a signature of the sea breeze or the orographically driven northeasterlies in the early evenings. Sturman and Tyson (1981) illustrated that the northeasterlies in Christchurch is initiated more frequently later in the day, especially in winter. The wind speed for RAD prefog periods is lower compared with other types of fog, indicating weak turbulence mixing.

A small number (approximately 15.7%) of EVP prefog periods show strong southwesterlies (wind speed greater than $4.0 \text{ m}\cdot\text{s}^{-1}$) (Figure 8e), which may indicate that the southwesterlies advect moisture to CHA in EVP events. The signal of the northeasterly flows also appears in EVP events. Despite the inadequate samples, most of the EVP events occurred in January and March (summer and

early autumn), while northeasterly is the dominant wind during summer as illustrated in (Sturman and Tyson, 1981). Figures 8e and 9e show a notable drop in wind speed from prefog periods to fog periods. Such drop is associated with reduction in turbulence mixing, which may be responsible for EVP formation.

CBL events are associated with a significant number of strong northeasterlies and a small number of southwesterlies, suggesting that clouds are pushed inland under the impact of synoptic-scale weather systems (Figure 8f). The high ratio of northeasterlies during CBL events suggests that the continuous input of clouds during CBL fog periods is mainly from the ocean. The ratio of northwesterlies during fog periods is greater than that during prefog periods in CBL events (Figure 9f). Similar to ADV–RAD and RAD events, the northeasterlies could be associated with a stable boundary layer suggesting the potential influence of boundary layer stability in CBL events.

FIGURE 7 The MSLP nearest to fog onset for each fog type: (a) all fog events, (b) ADV, (c) ADV-RAD, (d) RAD, (e) EVP, and (f) CBL. The average values of all events for each type are presented. The area between latitudes 25°–55°S and longitudes 160°E–175°W is chosen to represent the synoptic conditions as in Kidson (2000). The MSLP data are taken from the ERA5 data set (Hersbach *et al.*, 2019) [Colour figure can be viewed at wileyonlinelibrary.com]

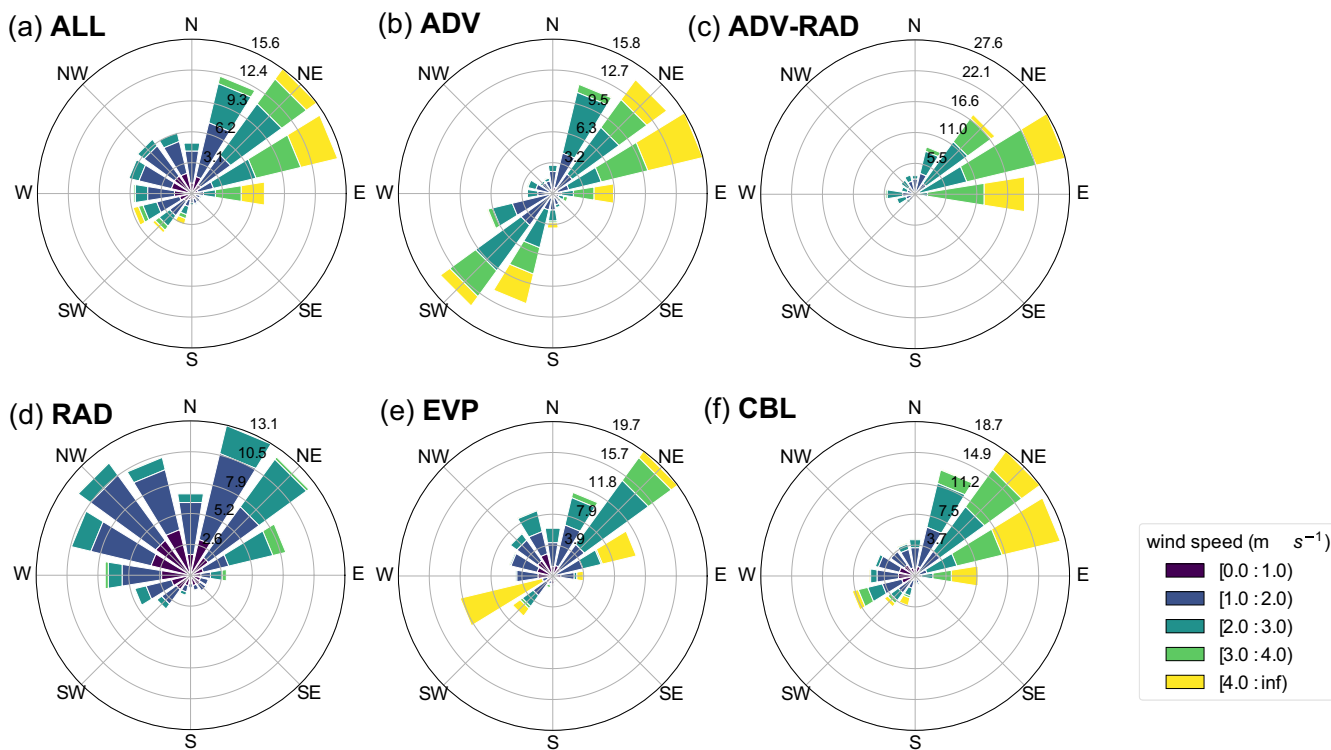
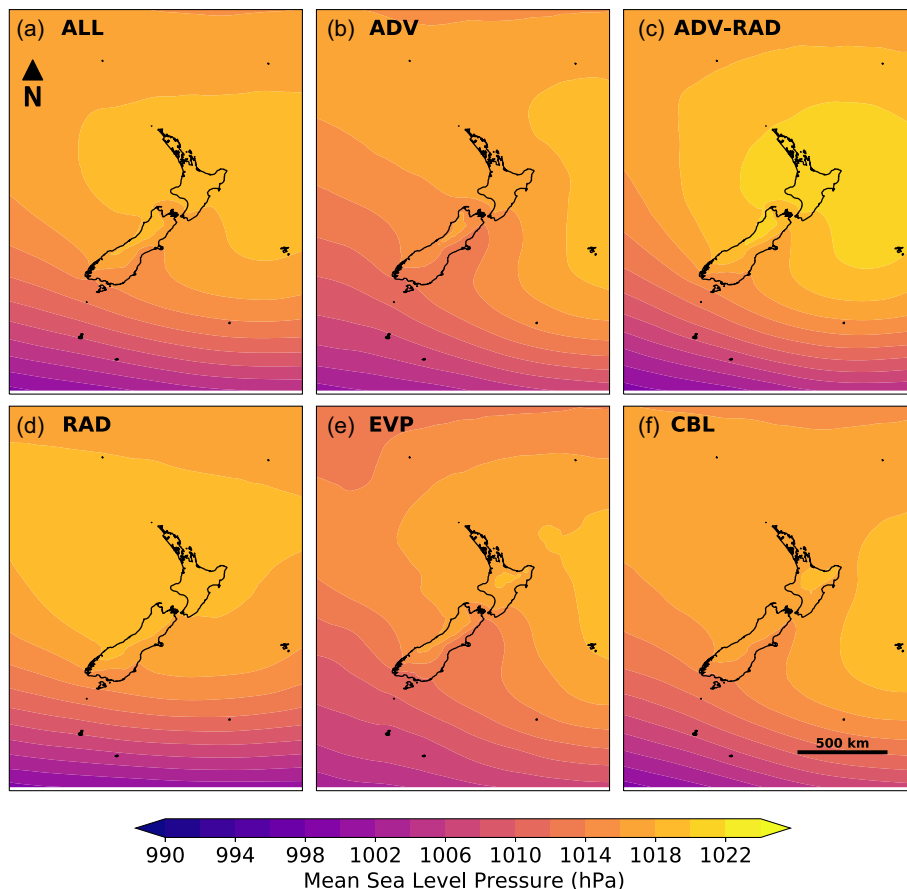


FIGURE 8 Wind roses of the 3-hr prefog periods for each fog type: (a) all fog events, (b) ADV, (c) ADV-RAD, (d) RAD, (e) EVP, and (f) CBL [Colour figure can be viewed at wileyonlinelibrary.com]

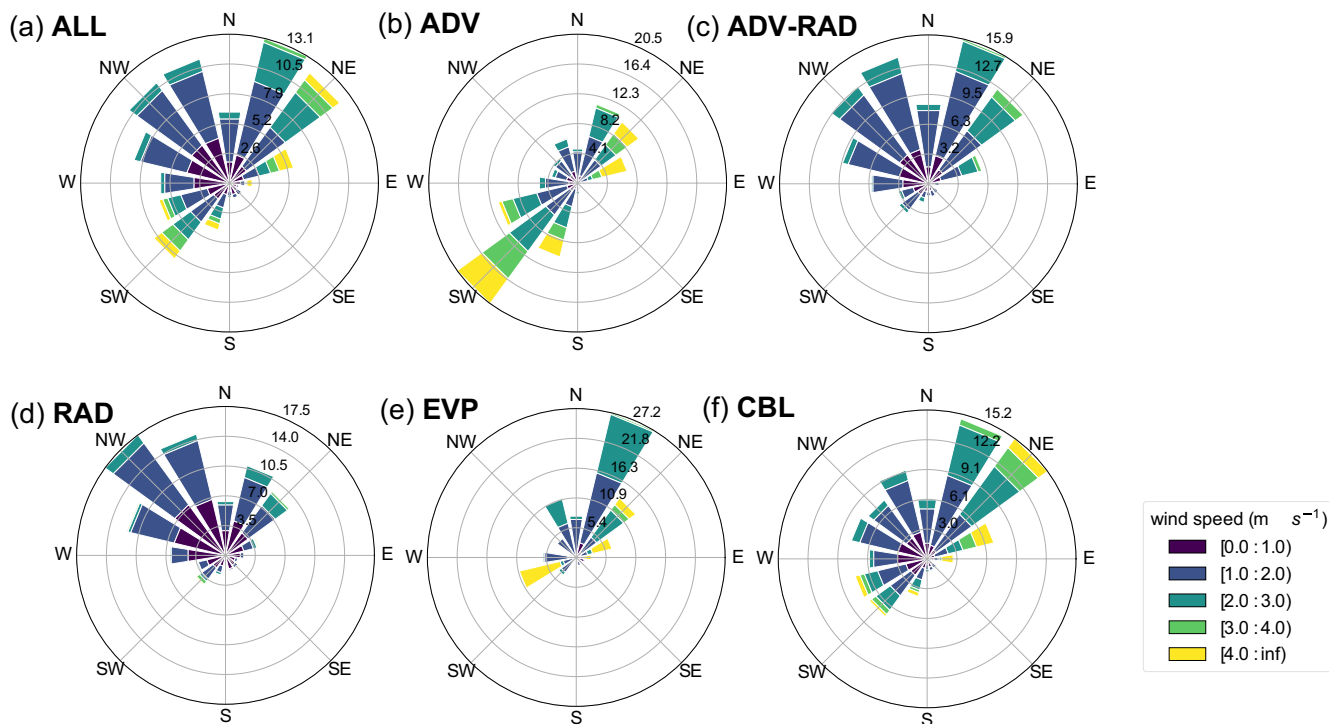


FIGURE 9 Similar to Figure 8, but for the fog periods [Colour figure can be viewed at [wileyonlinelibrary.com](https://onlinelibrary.wiley.com)]

5 | DISCUSSIONS AND CONCLUSIONS

In this study, we identified the climatological characteristics of fog at CHA over a 12-year period between 2007 and 2019. Fog events were identified using the 1-min visibility data obtained from the AWS at CHA. A novel quantitative method based on *MRI* was used to perform fog type classification of the identified fog events. In contrast to previous fog climatological studies (e.g., TR07; Akimoto and Kusaka, 2015; Bari *et al.*, 2016; Belorid *et al.*, 2015; Roux *et al.*, 2021; Van Schalkwyk and Dyson, 2013), the *MRI* method does not apply a fixed threshold to wind speed to distinguish different fog event types. Rather, the *MRI* (using temperatures and wind speed) was calculated to assess the dynamic stability of the near-surface layer in the atmosphere during prefog and fog periods. Based on that stability we classified fog events into different fog types. Also, the use of *MRI* overcomes the ambiguous descriptions of “cooling prior to onset” or “slight warming leading to onset” that was used in previous climatological studies to identify fog types.

Fog events were classified into five different types: ADV, ADV-RAD, RAD, EVP, and CBL. Fog characteristics are represented using the fog event duration, minimum visibility, diurnal and seasonal variability of fog occurrences. In addition, the synoptic and local wind flows at CHA during prefog and fog periods for each fog

type were examined. The climatological characteristics of each fog types found in this study are in agreement with climatological fog type studies at other sites around the world (e.g., TR07; Akimoto and Kusaka, 2015; Bari *et al.*, 2016; Belorid *et al.*, 2015; Roux *et al.*, 2021; Van Schalkwyk and Dyson, 2013). Overall, the results of fog characteristics show that ADV events have the longest duration, followed by CBL events. ADV events occur most frequently in August (late winter) associated with a relatively cool boundary layer and the lowest SST. Frequencies of ADV-RAD events peak in May and August, and most ADV-RAD events occurred during the second half of the evenings. Compared with other types of fog, ADV-RAD events have a relatively greater impact on reduction of visibility. RAD is the most common fog type at CHA, followed by CBL. EVP events are short-lived and their impact on visibility reduction is the least significant among all types of fog.

The presented results show that the *MRI* fog type classification method managed to capture the primary drivers to classify the ADV, ADV-RAD, and RAD events, while quantifying the criteria for fog type classification. In addition, the dynamic stability of both prefog and fog periods were considered, whereas the event-based method described in TR07 only focuses on the periods prior to or at fog onset. The *MRI* method has the potential to be applied to other regions where temperatures measurements at two different vertical levels, winds, and visibility

observations are available. When applying this method to data from other sites, the thresholds that categorize the strength of stability may change depending on the thickness of the measured layer. Extra care should be taken towards the unit of wind speed. Baker *et al.* (2002) and Syed *et al.* (2012) used knots, while our study uses $\text{m}\cdot\text{s}^{-1}$. Although the units do not alter the physical basis for *MRi* and its assessment of the dynamic stability, the values used for the *MRi* thresholds could vary. Due to the lack of fog type observations, the *MRi* method is only verified using the climatological characteristic results shown in section 4. Furthermore, only 13 EVP events were identified at CHA over the 12-year observational period. Such a low sample size may not be sufficient for a robust analysis of EVP events. In addition, due to the limitation of available data, only the local dynamic stability at CHA is assessed. Targeted fog type observations and/or field studies at multiple observational sites are required for future investigation of (a) verifying the *MRi* method further, and (b) comparing and combining the *MRi* method with TR07 to gain a better understanding of the processes involved in different fog types.

The classification of CBL events is mainly dependent on the observed cloud base height, which could be biased depending on the observation method. For example, in Bari *et al.* (2016), the cloud base height is determined by human observers, while our study uses cloud base height derived from ceilometer measurements. When fog forms at CHA, the ceilometer may record a sudden decrease of cloud base height from a few kilometres to a few hundred meters. This is commonly presented in ceilometer measurements (e.g., Nowak *et al.*, 2008; Arun *et al.*, 2018; An *et al.*, 2020), and different ceilometers may give different cloud layer measurements when fog occurs (e.g., Liu *et al.*, 2015). A more reliable classification for CBL events may be achieved by conducting case studies in numerical models to improve our understanding towards the relation between ceilometer observations and the processes involved in CBL events.

This study is the first to identify, classify, and analyse fog events at CHA using AWS data for a period over 10 years. The climatological study presented here aims to provide a general guidance of the characteristics of each fog type. This is a crucial first step of fog research at CHA which could aid forecasters' understanding of the processes and dynamics involved in local fog events. The results serve as a basis for more detailed fog research in the future. Future studies could investigate the application of climatological statistics in radiation fog forecast as described by Menut *et al.* (2014) and Román-Cascón *et al.* (2016). Further applications of *MRi* for fog forecasting as described by Baker *et al.* (2002) should be investigated in future field studies and/or with numerical weather prediction models and forecasters' guidance.

AUTHOR CONTRIBUTIONS

Dongqi Lin and Marwan Katurji participated on conceptualisation of the fog type classification methodology. Dongqi Lin developed the methodology, carried out formal analysis, investigation, and visualization, validated the fog event identification results, and wrote the original manuscript. Marwan Katurji, Laura Revell, Basit Khan, and Stefanie Kremser participated on continuous discussion of the analysis and manuscript. Stefanie Kremser, Laura Revell, and Marwan Katurji participated on the project and resources administration. Neal Osborne and Iman Soltanzadeh provided the MetService AWS data and participated on discussion of the methodology. All authors reviewed the manuscript.

ACKNOWLEDGEMENTS

Dongqi Lin, Laura E. Revell, and Stefanie Kremser received support from the University of Canterbury and the Ministry of Business, Innovation and Employment project Particulate Matter Emissions Maps for Cities (Grant No. BSCIF1802). The contribution of Basit Khan was supported by the MOSAIK and MOSAIK-2 projects, which are funded by the German Federal Ministry of Education and Research (BMBF) (Grant Nos. 01LP1601A and 01LP1911H), within the framework of Research for Sustainable Development (FONA; <http://www.fona.de>, last access: August 10, 2020). Marwan Katurji was supported by the Royal Society of New Zealand (Contract No. RDF-UOC1701). Open access publishing facilitated by University of Canterbury, as part of the Wiley - University of Canterbury agreement via the Council of Australian University Librarians.

DATA AVAILABILITY STATEMENT

New Zealand MetService maintains ownership of the raw AWS data and provided the data to the University of Canterbury on the understanding that it is for the purposes of fog research. The raw AWS data may not be used for commercial gain. The raw AWS data may not be made available to any third party, unless prior agreement has been obtained from MetService.

ORCID

Dongqi Lin  <https://orcid.org/0000-0003-3955-5882>

REFERENCES

- Akimoto, Y. and Kusaka, H. (2015) A climatological study of fog in Japan based on event data. *Atmospheric Research*, 151, 200–211. <https://doi.org/10.1016/j.atmosres.2014.04.003>.
- An, N., Pinker, R.T., Wang, K., Rogers, E. and Zuo, Z. (2020) Evaluation of cloud base height in the north american regional reanalysis using ceilometer observations. *International Journal of Climatology*, 40(6), 3161–3178.

- Arun, S., Sharma, S.K., Chaurasia, S., Vaishnav, R. and Kumar, R. (2018) Fog/low clouds detection over the Delhi earth station using the Ceilometer and the INSAT-3D/3DR satellite data. *International Journal of Remote Sensing*, 39(12), 4130–4144.
- Baker, R., Cramer, J. and Peters, J. (2002) *Radiation fog: UPS Airlines conceptual models and forecast methods*. Paper presented at 10th Conference on Aviation, Range, and Aerospace Meteorology.
- Bari, D., Bergot, T. and El Khelifi, M. (2016) Local meteorological and large-scale weather characteristics of fog over the Grand Casablanca region, Morocco. *Journal of Applied Meteorology and Climatology*, 55(8), 1731–1745.
- Belorid, M., Lee, C.B., Kim, J.-C. and Cheon, T.-H. (2015) Distribution and long-term trends in various fog types over South Korea. *Theoretical and Applied Climatology*, 122(3), 699–710.
- Bergot, T., Escobar, J. and Masson, V. (2015) Effect of small-scale surface heterogeneities and buildings on radiation fog: large-eddy simulation study at Paris-Charles de Gaulle airport. *Quarterly Journal of the Royal Meteorological Society*, 141(686), 285–298. <https://doi.org/10.1002/qj.2358>.
- Colby, F.P. (1998) A preliminary investigation of temperature errors in operational forecasting models. *Weather and Forecasting*, 13(1), 187–205.
- Corsmeier, U., Kossmann, M., Kalthoff, N. and Sturman, A. (2006) Temporal evolution of winter smog within a nocturnal boundary layer at Christchurch, New Zealand. *Meteorology and Atmospheric Physics*, 91, 129–148. <https://doi.org/10.1007/s00703-005-0111-5>.
- Dupont, J.-C., Haeffelin, M., Protat, A., Bouniol, D., Boyouk, N. and Morille, Y. (2012) Stratus-fog formation and dissipation: a 6-day case study. *Boundary-Layer Meteorology*, 143(1), 207–225.
- Environment Canterbury Regional Council. (2020) Christchurch and ashley river, canterbury, new zealand 2018. <https://doi.org/10.5069/G91J97WQ>.
- George, J.J. (1951) Fog. In: Malone, T.F. (Ed.) *Compendium of Meteorology: Prepared under the Direction of the Committee on the Compendium of Meteorology*. Boston, MA: American Meteorological Society, pp. 1179–1189.
- Gultepe, I., Tardif, R., Michaelides, S.C., Cermak, J., Bott, A., Bendix, J., Müller, M.D., Pagowski, M., Hansen, B., Ellrod, G., Jacobs, W., Toth, G. and Cober, S.G. (2007) Fog research: a review of past achievements and future perspectives. *Pure and Applied Geophysics*, 164(6–7), 1121–1159. <https://doi.org/10.1007/s00024-007-0211-x>.
- Hersbach, H., Bell, B., Berrisford, P., Horányi, A., Sabater, J.M., Nicolas, J., Radu, R., Schepers, D., Simmons, A. and Soci, C. (2019) Global reanalysis: goodbye ERA-Interim, hello ERA5. *ECMWF Newsletter*, 159, 17–24.
- Hume, T. (1999) *Fog at New Zealand Airports*. PhD thesis, Victoria University of Wellington.
- ICAO. (2018) *Meteorological Service for International Air Navigation: Annex 3 to the Convention on International Civil Aviation*. Montreal, QC: International Civil Aviation Organization.
- Kidson, J.W. (2000) An analysis of New Zealand synoptic types and their use in defining weather regimes. *International Journal of Climatology: A Journal of the Royal Meteorological Society*, 20(3), 299–316.
- Kossmann, M. and Sturman, A. (2004) The surface wind field during winter smog nights in Christchurch and coastal Canterbury, New Zealand. *International Journal of Climatology*, 24(1), 93–108.
- Land Information New Zealand. (2021) Christchurch 0.075m urban aerial photos (2015–2016). Available at: <https://data.linz.govt.nz/layer/53451-christchurch-0075m-urban-aerial-photos-2015-2016/> [Accessed on 27th August 2021].
- Landcare Research. (2018) Nzdem south island 25 metre. Available at: <https://lris.scinfo.org.nz/layer/48127-nzdem-south-island-25-metre/> [Accessed on 27th July 2021].
- Landcare Research. (2020a) Nzdem north island 25 metre. Available at: <https://lris.scinfo.org.nz/layer/48131-nzdem-north-island-25-metre/> [Accessed on 27th July 2021].
- Landcare Research. (2020b) Lcdb v5.0-land cover database version 5.0, mainland New Zealand. Available at: <https://lris.scinfo.org.nz/layer/104400-lcdb-v50-land-cover-database-version-50-mainland-new-zealand/> [Accessed on 23rd April 2021].
- Liu, D., Yan, W., Yang, J., Pu, M., Niu, S. and Li, Z. (2016) A study of the physical processes of an advection fog boundary layer. *Boundary-Layer Meteorology*, 158(1), 125–138.
- Liu, L., Sun, X.-J., Liu, X.-C., Gao, T.-C. and Zhao, S.-J. (2015) Comparison of cloud base height derived from a ground-based infrared cloud measurement and two ceilometers. *Advances in Meteorology*, 2015, 1–8.
- Macara, G.R. (2016) *The Climate and Weather of Canterbury*. Wellington, New Zealand: NIWA.
- Maronga, B. and Bosveld, F. (2017) Key parameters for the life cycle of nocturnal radiation fog: a comprehensive large-eddy simulation study. *Quarterly Journal of the Royal Meteorological Society*, 143(707), 2463–2480.
- Mazoyer, M., Lac, C., Thouron, O., Bergot, T., Masson, V. and Musson-Genon, L. (2017) Large eddy simulation of radiation fog: impact of dynamics on the fog life cycle. *Atmospheric Chemistry and Physics*, 17(21), 13017–13035.
- McKendry, I.G. (1983) Spatial and temporal aspects of the surface wind regime on the Canterbury plains, New Zealand. *Journal of Climatology*, 3(2), 155–166.
- Menut, L., Mailler, S., Dupont, J.-C., Haeffelin, M. and Elias, T. (2014) Predictability of the meteorological conditions favourable to radiative fog formation during the 2011 ParisFog campaign. *Boundary-Layer Meteorology*, 150(2), 277–297.
- Nowak, D., Ruffieux, D., Agnew, J.L. and Vuilleumier, L. (2008) Detection of fog and low cloud boundaries with ground-based remote sensing systems. *Journal of Atmospheric and Oceanic Technology*, 25(8), 1357–1368.
- Oke, T.R. (2002) *Boundary Layer Climates*. Oxfordshire, UK: Routledge.
- Pilié, R.J., Mack, E.J., Kocmond, W.C., Rogers, C.W. and Eadie, W.J. (1975) The life cycle of valley fog. Part I: micro-meteorological characteristics. *Journal of Applied Meteorology*, 14(3), 347–363.
- Price, J. (2011) Radiation fog. Part I: observations of stability and drop size distributions. *Boundary-Layer Meteorology*, 139(2), 167–191.
- Román-Cascón, C., Steeneveld, G.J., Yagüe, C., Sastre, M., Arrillaga, J.A. and Maqueda, G. (2016) Forecasting radiation fog at climatologically contrasting sites: evaluation of statistical methods and WRF. *Quarterly Journal of the Royal Meteorological Society*, 142(695), 1048–1063.

- Roux, B., Potts, R., Siems, S. and Manton, M. (2021) Towards a better understanding of fog at Perth Airport. *Journal of Hydrology*, 600, 126–516. <https://doi.org/10.1016/j.jhydrol.2021.126516>.
- Ryznar, E. (1977) Advection-radiation fog near Lake Michigan. *Atmospheric Environment*, 11(5), 427–430.
- Smith, D., Renfrew, I., Price, J. and Dorling, S. (2018) Numerical modelling of the evolution of the boundary layer during a radiation fog event. *Weather*, 73(10), 310–316.
- Sturman, A.P. and Tapper, N.J. (2006) *The Weather and Climate of Australia and New Zealand*. Oxford: Oxford University Press.
- Sturman, A.P. and Tyson, P.D. (1981) Sea breezes along the Canterbury coast in the vicinity of Christchurch, New Zealand. *Journal of Climatology*, 1(3), 203–219.
- Syed, F.S., Körnich, H. and Tjernström, M. (2012) On the fog variability over South Asia. *Climate Dynamics*, 39(12), 2993–3005. <https://doi.org/10.1007/s00382-012-1414-0>.
- Tardif, R. and Rasmussen, R.M. (2007) Event-based climatology and typology of fog in the New York City region. *Journal of Applied Meteorology and Climatology*, 46(8), 1141–1168.
- Van Schalkwyk, L. and Dyson, L.L. (2013) Climatological characteristics of fog at Cape Town International airport. *Weather and Forecasting*, 28(3), 631–646.
- Willett, H.C. (1928) Fog and haze, their causes, distribution, and forecasting. *Monthly Weather Review*, 56, 435–468.
- WMO. (1992) *International meteorological vocabulary*. Geneva: WMO. Technical report: WMO/OMM/IMGW, p. 182.
- Zhang, J.-W., Xue, H.-W., Deng, Z.-Z., Zhao, C.-S. and Zhang, Q.-H. (2013) Effects of aerosols on fogs observed in the North China Plain. *Atmospheric and Oceanic Science Letters*, 6(2), 79–83.

How to cite this article: Lin, D., Katurji, M., Revell, L. E., Khan, B., Osborne, N., Soltanzadeh, I., & Kremser, S. (2022). Fog type classification using a modified Richardson number for Christchurch, New Zealand. *International Journal of Climatology*, 1–17. <https://doi.org/10.1002/joc.7761>